

Characteristics analysis of moon-based earth observation under the ellipsoid model

Liu, Guang; Guo, Huadong; Hanssen, Ramon F.

DOI

[10.1080/01431161.2020.1797220](https://doi.org/10.1080/01431161.2020.1797220)

Publication date

2020

Document Version

Final published version

Published in

International Journal of Remote Sensing

Citation (APA)

Liu, G., Guo, H., & Hanssen, R. F. (2020). Characteristics analysis of moon-based earth observation under the ellipsoid model. *International Journal of Remote Sensing*, 41(23), 9121-9139.
<https://doi.org/10.1080/01431161.2020.1797220>

Important note

To cite this publication, please use the final published version (if applicable).
Please check the document version above.

Copyright

Other than for strictly personal use, it is not permitted to download, forward or distribute the text or part of it, without the consent of the author(s) and/or copyright holder(s), unless the work is under an open content license such as Creative Commons.

Takedown policy

Please contact us and provide details if you believe this document breaches copyrights.
We will remove access to the work immediately and investigate your claim.



Characteristics analysis of moon-based earth observation under the ellipsoid model

Guang Liu ^a, Huadong Guo ^a and Ramon F. Hanssen ^b

^aKey Laboratory of Digital Earth Sciences, Institute of Remote Sensing and Digital Earth, Chinese Academy of Sciences, Beijing, China; ^bDepartment of Geodesy and Satellite Earth Observation, Delft University of Technology, Delft, The Netherlands

ABSTRACT

Using the Moon as an Earth observation platform for remote sensing offers the benefits of a high orbital altitude and vast surface area, which could provide continuous Earth observation capabilities over great temporal and spatial scales. Over the course of China's follow-up lunar missions in the next three Five-year plans, the Earth observation instruments will be put on the Moon. However, the understanding of the characteristics of Moon-based Earth observations remains limited. Here, the observational characteristics for a moon-based platform related to the Earth ellipsoid model is studied, which advances previous studies with a spherical Earth assumption. We perform three analyses. First, an integrated coordination transformation equation, which denotes the geometric relationship between a Moon-based platform and the target on Earth is established based on numerical ephemerides and Earth orientation parameters. Second, the explicit expression for the intersection between the line of sight of the sensor and the Earth oblate spheroid is formulated, and the formulae of uncertainties are given. Lastly, a theoretical visible area on the Earth ellipsoid observed from the sensor is derived based on the geometrical relationship between the observation position and the Earth ellipsoid; two special situations are obtained via explicit expressions and series expansion. Based on this, the optimum radius for the spherical assumption of the Earth is obtained. The simulation and analyses reveal that the proposed mathematical derivation aimed at the Earth spheroid can be used to improve the accuracy of studies focused on the geometrical characteristics of Moon-based Earth observations.

ARTICLE HISTORY

Received 13 January 2020
Accepted 26 April 2020

1. Introduction

Since the later part of the past century, Earth observation techniques, which utilize remote sensors to observe targets on Earth, have been used in many fields, including forestry, oceanography, and polar studies (Ryerson 1998; Sandau 2010). To this end, various artificial platforms, such as balloons, air planes, Earth orbit satellites, space shuttles, space stations, and Lagrange point vehicles have been developed for Earth observation

CONTACT Guang Liu  liuguang@radi.ac.cn  Key Laboratory of Digital Earth Sciences, Institute of Remote Sensing and Digital Earth, Chinese Academy of Sciences, Beijing 100094, China
 Supplemental data for this article can be accessed [here](#).

(Herman et al. 1986; Vömel 2002; Lautenbacher 2006; Sandau 2010; Guo et al. 2016aa). These Earth observation techniques have provided numerous datasets that aided our understanding of planet Earth (Andrew 2015; Chuvieco 2008; Stammer and Cazenave 2017; Jiang and Shekhar 2017). In recent years, as Earth system sciences have advanced, the need to monitor the Earth with both temporal consistency and spatial continuity to study the Earth system as a whole and understand global problems, especially climate change, has increased (Rosenqvist et al. 2010; Reid et al. 2010; Skinner and Murck 2011; Ryu and Hayhoe 2017).

The Moon is the largest and only natural satellite of the Earth, and it is the only place other than Earth where humans have been. Since the 1950s, there have been more than 100 lunar missions (May 2017). Recently, with the rapid advancement of aerospace technologies and increasing interest in the Moon, a Moon-based Earth observation platform has been proposed (Guo et al. 2016b; Liu et al. 2016) as one part of future lunar missions. Compared with air-borne and space-borne satellites, Moon-based Earth observations have three unique characteristics (Liu et al. 2016; Ren et al. 2017a): (1) The Moon's rotational period is the same as the orbital period around the Earth. The distance from the Moon to the Earth is about 380,000 km; therefore, installing sensors with a small field of view (FOV) on the nearside of the Moon could allow us to observe the whole Earth disk (Bendek et al. 2015; Stahl 2017) with temporal consistency and spatial continuity. (2) The Moon is the largest and only natural satellite of the Earth, with a diameter about 3,500 km (May 2017), and various sensors could be installed to simultaneously obtain information on the Earth from space to the subsurface, which could improve our understanding of the Earth's dynamic systems. (3) The Moon has a stable geological environment (Taylor 1988; Blair et al. 2017), and it, thus, offers the opportunity to instal advanced sensor groups with stable baselines and geometric configurations.

Previous lunar missions that orbited, passed over, or landed on the Moon have already demonstrated the feasibility to observe the Earth from the Moon. The first panoramic photo of the Earth was taken when the United States National Aeronautics and Space Administration (NASA) launched the 'Lunar Orbiter' in 1966. The Lunar Orbiter travelled around the Moon (<https://lunar.gsfc.nasa.gov>), and in 1972, during the Apollo 16 mission, a 75 mm diameter Schmidt telescope with far ultraviolet bandwidth was placed in the shadow of the lunar module, and photos of the Earth's upper atmosphere, including airglow and aurorae, were obtained (G. R. Carruthers and Page 1972, 1976). More recently, the world has experienced a new wave of lunar exploration and development, including the Selenological and Engineering Explorer mission of Japan, the Lunar Reconnaissance Orbiter mission and Deep Space Gateway of NASA, the Small Missions for Advanced Research in Technology-1 (SMART-1) mission of the European Space Agency (ESA), and the Chinese Lunar Exploration Program. These missions have used sensors with different wavelengths, including both visible and ultraviolet wavelengths to take valuable photos of the Earth (Muinonen et al. 2002; Zheng et al. 2008; Yamazaki et al. 2010). Due to the unique characteristics of Moon-based Earth observations, the NASA organized a Lunar Earth observatory workshop in 2006 (NASA 2006; P Hamill 2007; Johnson et al. 2007); ten years later, a special session on Moon-based Earth observation was held at the 2016 International Geoscience and Remote Sensing Symposium, where scientists from China, the United States, and Europe discussed new perspectives and future research priorities

(Guo et al. 2016b ; Renga and Moccia 2016; Patrick Hamill 2016; Huang et al. 2016; Kaufmann and Song 2016; Ye et al. 2016; Ren et al. 2016).

Early after the Moon-based Earth observation workshop, several researchers considered the feasibility of Moon-based Earth observations. Palle et al. proposed to observe the surface albedo of the Earth with visible and thermal infrared sensors (Pallé and Goode 2009). Guo proposed exploring Earth observation systems consisting of multiple platforms, including the Moon, satellites, aircrafts, and land-based sensors (Guo 2009). Moccia et al. studied the potential of Moon-based Synthetic Aperture Radar (SAR) sensors to observe the Earth and proposed different configurations of SAR systems (Moccia and Renga 2010; Fornaro et al. 2010). Zhang studied the observation geometry of Moon-based Earth observations, and discussed simulation technologies based on the Jet Propulsion Laboratory (JPL) ephemerides (Zhang 2012). Many more studies were conducted after the IGARSS 2016. Liu et al. studied the potential of Moon-based observations for studying large-scale geological phenomena, and proposed the construction of a Moon-based Earth Observation System (Liu et al. 2016). Guo et al. further proposed the installation of a Moon-based SAR system to monitor global climate change (Guo, Liu, and Ding 2017). An international effort to further develop the theory behind Moon-based Earth observations was proposed by Song and colleagues (Song et al. 2017). Observation geometry for SAR based on a semi-analytic model and assumptions that both the Earth and the Moon are spherical was introduced by Moccia and Renga (Moccia and Renga 2010). Fornaro et al. used a simplified Keplerian six-parameter Moon orbital model to further develop the observation geometry of SAR sensors. Ren et al. proposed an observation geometric model for lunar electro-optical region observation, which included the coordination system transformation from the principal axis lunar reference system (PALRS) to the international terrestrial reference system (ITRS), together with the usage of Jet Propulsion Laboratory numerical ephemerides 430 (DE430) and considering the polar motion deal with Earth orientation parameters (EOP) for the first time (Ren et al. 2017b). Based on Ren's work, several studies were presented concerning Moon-based Earth observation geometry, the analysis of effective coverage and the scope of observation, the signal model of Moon-based SAR, and other applications (Ye et al. 2018a, 2018; Xu and Chen 2019; Ding et al. 2019; Xu, Chen, and Zhou 2019; Wu et al. 2020). All these studies have provided valuable insights for Moon-based Earth observations.

Although the assumption of sphericity has been used in previous studies to simplify the geometry models for Moon-based Earth observations, there are few studies that have defined the criteria for the optimum spherical radius of the Earth for specific phenomena, such as the visible area that is related to the position of the sensor and the radius of the sphere. Furthermore, for most geological applications, the Earth is considered as an ellipsoid, such as that used in the Geodetic Reference System 1980 (GRS 80), instead of a sphere. Thus, this study has three main contributions. The first is to introduce an integrated coordination transformation equation, which forms the observation geometry between the Moon-based sensor and the target on Earth, and is different from the equations used in previous studies (Moccia and Renga 2010; Zhang 2012; Ren et al. 2017a; Ding et al. 2019) that used step-wise transformations between the main coordination systems. For example, Ye et al. proposed an equation for coordination transformation (Ye et al. 2018b); however, their transformation matrix \mathbf{T} did not have a real physical meaning. The second

contribution of this study is the addition of an explicit expression for the intersection between the line of sight (LOS) of the sensor and the modelled Earth ellipsoid to the integrated coordination transformation equation, and the provision of sensitive factors between the position components relative to the LOS vector components. Sensor position components are derived and expressed in the supplemental material in close-form. The third contribution is the derivation of the visible area for an ellipsoid from remote sensors. An explicit expression is provided for sensors located on the polar axis, while a series expansion method is used for sensors on the equatorial plan. A distance-related optimum radius of the Earth is finally obtained.

The remainder of this paper is organized as follows: [Section 2](#) first introduces the coordination system transformation for Moon-based Earth observation and the integrated coordination transformation equation based on the JPL ephemerides and Earth orientation information. Then, the explicit expression of the intersection between LOS and the Earth ellipsoid is derived based on the geometrical relationship between the Moon and the Earth. Formulae are derived for two special cases of the visible area on the modelled Earth ellipsoid observed by the sensors. [Section 3](#) presents the simulations and analyses based on the developed mathematical formulae. The temporal and spatial distributions of sensitive factors are then simulated and analysed, and the optimum radius for visible area research is written as a function of the distance between the Earth and the Moon. Finally, we discuss our findings, including sources of error in this study, and aims for future studies are provided in [Section 4](#).

2. Data and theory

The regular method of studying the characteristics of Earth observations is to place sensors and targets into the same coordinate system. The relative position of the Earth and the Moon will determine the Moon-based earth observation geometry, and it is a common situation for the position of targets on Earth to be defined in the geodetic coordinate system of the Earth, while the positions of sensors on the Moon are defined in the geodetic coordinate system of the Moon. These two coordinate systems are both body-centred and body-fixed coordinate systems, and coordinate system transformation is needed for studying Earth observations from the Moon. Another issue is the shape of the Earth, i.e., the assumption of a spherical Earth is simple. Under this assumption, the entire Earth is shaped as a sphere, and the geometry of Moon-based Earth observation is very simple, which has been obtained in other studies (Fornaro et al. 2010; Ren et al. 2017a; Ye et al. 2017; Xu and Chen 2018). However in geodesy, the Earth is always represented as an ellipsoid, which is obtained by rotating an ellipse around its shorter axis (Clarke 1878; Ikeda and Dobson 1995; Goodchild et al. 2012). The related observation geometry based on an ellipsoid model is studied in this work.

2.1. Coordination transformation for moon-based earth observation

Coordination system transformation is the basis for studying Earth observation from the Moon. Several studies related to the transformation of the Moon-based Earth observation coordination system have been conducted using a separated coordination transformation

(Moccia and Renga 2010; Ren et al. 2017a; Ding et al. 2019). The following section will introduce an integrated transformation, considering that JPL Development Ephemeris (DE) series are the most popular ephemerides, which include the positions of the Earth and the Moon (Folkner, Williams, and Boggs 2009). The JPL DE data were used as described in (Ren et al. 2017a) to implement the integrated transformation. Figure 1 depicts the relationships of the coordination system transformation and the transformation vector. The vector S points to the sensor on the Moon which is obtained from the attitude parameters of the Moon and the Moon's centre position, while the vector T points to the target on Earth which is obtained from the Earth Orientation Parameters and the Earth's position.

The positions of targets on Earth are defined in the geodetic coordinate system of the Earth, whereas the positions of sensors on the Moon are defined in the lunar geodetic coordinate system. For the position vector on Earth in the geodetic coordinate system, it is simple to transform it into the International Terrestrial Reference System (ITRS) coordinate system, which is expressed as the sum of trigonometric functions for longitude and latitude, written here as $P_{ITRS}^{target}(x, y, z)$, where x , y , and z are the coordinates along the x -, y -, and z -axes in the ITRS coordination system, respectively. There have been many studies on this matter (Jekeli 2001; Seeber 2003; Torge and Müller 2012), and nearly the same position vector may be used to transform the coordinates on the Moon from the lunar geodetic coordinate system into the Moon-centred, body-fixed coordinate system (MCMF), first the Mean Earth (ME) coordinate system, written as: $P_{ME}^{sensor}(x, y, z)$. The workflow for transforming the position vector $P_{ME}^{sensor}(x, y, z)$ on the ME coordinate system to the ITRS coordinate system is complex (Figure 2); there are eight main transformation steps. Assuming the position vector of the sensor $P_{ME}^{sensor}(x, y, z)$ was transformed into the ITRS Earth-centred, body-fixed coordinate system, and its position vector in the ITRS coordinate system is $P_{ITRS}(x, y, z)$, then the integrated expression may be written as:

$$P_{ITRS}(x, y, z) = \mathbf{WRNPB} (L + \mathbf{V} \mathbf{U} P_{ME}(x, y, z)) \quad (1)$$

The constant matrix \mathbf{U} represents the transformation from the ME system to the principal axis (PA) system, which was defined by (Archinal et al. 2011). The matrix \mathbf{V} represents the

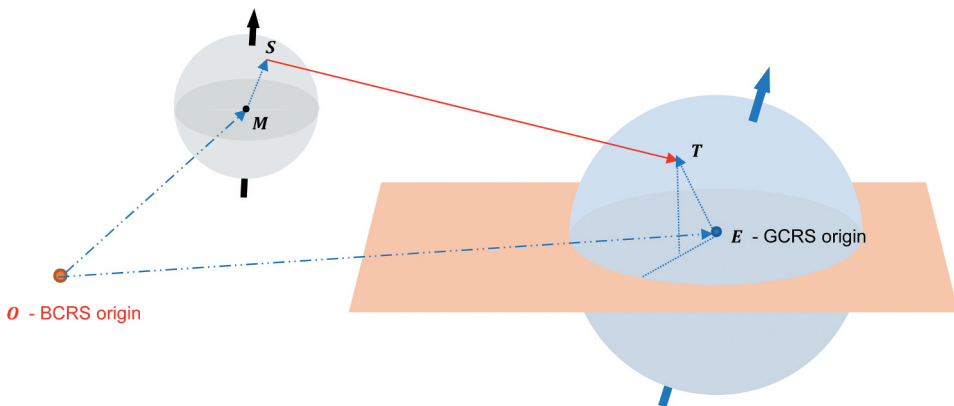


Figure 1. Schematic of the relationships for the coordinate system transformation for moon-based earth observations.

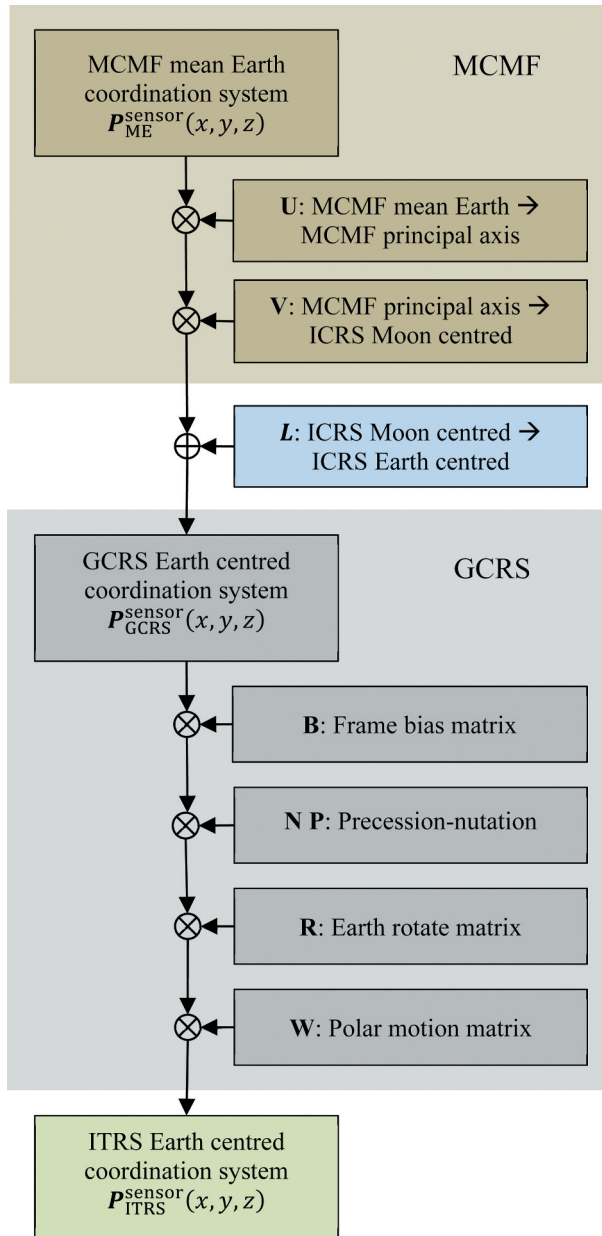


Figure 2. Transformation chain workflow for the position vectors of a moon-based sensor in the Mean Earth (ME) coordinate system into the International Terrestrial Reference System (ITRS) earth-centred coordinate system.

transformation from the PA system to the International Celestial Reference System (ICRS) Moon-centred system with three Euler angles, and the vector *L* represents the offset between the ICRS Earth-centred system to the ICRS Moon-centred system, which were defined by IERS Conventions (Folkner, Williams, and Boggs 2009). The matrix **B** represents the frame bias between the equinox (J2000.0) and the Geocentric Reference System

(GCRS). The matrices \mathbf{P} , \mathbf{N} , and \mathbf{R} reflect the characteristics of the precession, nutation, and rotation of the Earth separately, and they are defined in (McCarthy and Petit 2004). The matrix \mathbf{W} represents the polar motion, which corresponds to the kinematic definition of the non-rotating origin in the ITRS when the Celestial Intermediate Pole (CIP) is moving with respect to the ITRS (McCarthy and Petit 2004). With the integrated transformation, the sensor on the Moon and the target on Earth could be put into the same ITRS Cartesian coordinate system. The position of the Sun was transformed to the same ITRS Cartesian coordinate system using a similar procedure.

2.2. Geometry analyses for moon-based earth observation

After the coordinate system transformation, the position vectors of the sensor on the Moon $P_{ITRS}^{sensor}(x, y, z)$, the target on Earth $P_{ITRS}^{target}(x, y, z)$, and the Sun $P_{ITRS}^{sun}(x, y, z)$ were in the same ITRS Cartesian coordinate system. For simplicity, they are written as: $p^{sensor}(x, y, z)$, $p^{target}(x, y, z)$, and $p^{sun}(x, y, z)$, respectively. As mentioned previously, the Earth is commonly modelled as an ellipsoid E (Moritz 1980; Chovitz 1981; Grafarend, Klapp, and Martinec 2010); here we assume the target is located on the surface of

$$\frac{x^2}{a^2} + \frac{y^2}{a^2} + \frac{z^2}{b^2} = 1 \quad (2)$$

where x , y , and z are the coordination variables on the ITRS system, and a and b are the length of the semi-major (equator) and semi-minor (polar) axes of the spheroid.

The LOS of the sensor is important in Earth observations as it represents the observation direction of the sensor. Assuming the sensor is located at the point $p = (x_p, y_p, z_p)$ outside of ellipsoid E , where x_p , y_p , and z_p are the components of the position of the sensor within the coordinate system, the LOS unit vector is $\hat{l} = (m, n, q)$, where m , n , and q are components of the LOS unit vector, and the target $t = (x_t, y_t, z_t)$ is the intersection point between the LOS vector and the ellipsoid surface. The explicit expression for t can then be obtained by direct calculation via the equation of the line through the point p with the direction vector along LOS \hat{l} . It is common for the LOS vector to intersect the ellipsoid E , and it will have two solutions

$$t = p - \left[(\hat{l} \circ e) \cdot (p \circ e) \pm \sqrt{((\hat{l} \circ e) \cdot (p \circ e))^2 - \hat{l} \circ e^2 (\|p \circ e\|^2 - 1)} \right] \frac{\hat{l}}{\|\hat{l} \circ e^2\|} \quad (3)$$

where \cdot is the dot product, \circ is the Handmaid product, $\|\cdot\|$ is the norm of a vector, and $e = (1/a, 1/a, 1/b)$ represents the geometric parameters of the ellipsoid E . Equation (3) gives the explicit expression of the position vector of the intersection point $t = (x_t, y_t, z_t)$ from a sensor looking at an ellipsoid. This expression shows that the position vector is determined by the LOS vector, ellipsoid geometry parameters, and the location of the sensor. The uncertainties of the location of the sensor and LOS vector will propagate into the position vector. Using Equation (3), the relationship among the uncertainties of $t = (x_t, y_t, z_t)$, the uncertainties of the sensor position $p = (x_p, y_p, z_p)$, and the LOS vector $\hat{l} = (m, n, q)$ are related via Equation (4) and Equation (5), where J_p and are the matrix of

sensitive factors and the definitions of the components of the matrixes are presented in the supplemental material.

$$\mathbf{J}_p = \begin{bmatrix} \frac{\partial t_x}{\partial p_x} & \frac{\partial t_x}{\partial p_y} & \frac{\partial t_x}{\partial p_z} \\ \frac{\partial t_y}{\partial p_x} & \frac{\partial t_y}{\partial p_y} & \frac{\partial t_y}{\partial p_z} \\ \frac{\partial t_z}{\partial p_x} & \frac{\partial t_z}{\partial p_y} & \frac{\partial t_z}{\partial p_z} \end{bmatrix} \quad (4)$$

$$\mathbf{J}_i = \begin{bmatrix} \frac{\partial t_x}{\partial l_x} & \frac{\partial t_x}{\partial l_y} & \frac{\partial t_x}{\partial l_z} \\ \frac{\partial t_y}{\partial l_x} & \frac{\partial t_y}{\partial l_y} & \frac{\partial t_y}{\partial l_z} \\ \frac{\partial t_z}{\partial l_x} & \frac{\partial t_z}{\partial l_y} & \frac{\partial t_z}{\partial l_z} \end{bmatrix} \quad (5)$$

Commonly, there are two intersection points between the LOS vector and the ellipsoid Earth; if these two intersection points shrink into one point, then the LOS vector is tangent to the Earth ellipsoid surface. All resulting tangent points $t = (x_t, y_t, z_t)$, with respect to the sensor position $p = (x_p, y_p, z_p)$, are located on the same plane, and fulfil

$$\frac{x_t x_p}{a^2} + \frac{y_t y_p}{a^2} + \frac{z_t z_p}{b^2} = 1 \quad (6)$$

The visible area on Earth from the sensor located on the Moon is presented in [Figure 3](#). Although the moon is far away from the Earth, it is still a finite distance, and the visible area is not half of the Earth’s surface. Under normal conditions, for a surface in three-dimensional (3D) space, which is defined by $z = z(x, y)$, the visible surface area in a rectangular Cartesian coordinate system can be written as standard double integrals formula, as in (Harris and Stocker 1998). For a standard ellipsoid, the integration of the surface area was derived by Cotes (Gowing 1983) using [Equation \(7\)](#), where $\varepsilon = \sqrt{a^2 - b^2}/a$ is the eccentricity of the Earth ellipsoid, which is about 0.08 in the GRS 80.

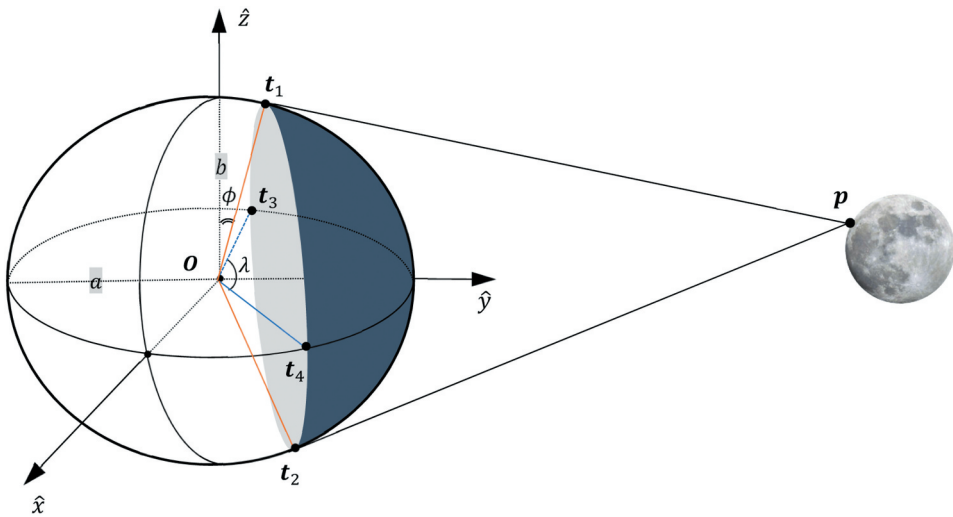


Figure 3. The visible area on the earth from the moon-based sensor. Due to the finite distance between the earth and the moon, the visible area is not half of the earth’s surface.

Although the total area of an ellipsoid can be explicitly expressed, it is not yet possible to obtain an explicit expression for the visible area of specific parts of the Earth under most conditions.

$$S_{\text{surface}} = \pi \left[2a^2 + \frac{b^2}{\varepsilon} \ln \left(\frac{1 + \varepsilon}{1 - \varepsilon} \right) \right] \quad (7)$$

However, there are two extreme situations in which the visible area may be explicitly obtained. The first situation is when the sensor is located on the equatorial plane, and the visible area may be expressed as

$$S_{\text{visible}}^{\text{equator}} = 4a^2 \int_0^{a/D_{\text{ME}}} \sqrt{1 - \varepsilon^2 x^2} \text{EllipticE} \left[\frac{1 - x^2}{1/\varepsilon^2 - x^2} \right] dx \quad (8)$$

where $\varepsilon = \sqrt{a^2 - b^2}/a$ is the eccentricity of the Earth ellipsoid, D_{ME} is the distance from the sensor to the centre of the Earth and the visible area could be obtained with series expansion, $\text{EllipticE}[\cdot]$ is the complete elliptic integral. It is clear that the visible area of the reference ellipsoid of the Earth from the sensor located on the equatorial plane is a function of eccentricity, the length of the semi-major and semi-minor axes of the ellipsoid, and the distance between the centre of the Earth and the Moon. Another situation, in which the total visible area may be explicitly expressed, is when the sensor is located on the polar axis; in this case, the visible area may be expressed as

$$S_{\text{visible}}^{\text{polar}} = \pi a^2 \left(1 - \sin \theta_2 \sqrt{1 - \varepsilon^2 \cos^2 \theta_2} \right) + \frac{\pi b^2}{\varepsilon} \ln \left[\frac{1 + \varepsilon}{\varepsilon \sin \theta_2 + \sqrt{1 - \varepsilon^2 \cos^2 \theta_2}} \right] \quad (9)$$

where $\varepsilon = \sqrt{a^2 - b^2}/a$ is the eccentricity of the Earth ellipsoid, and $\theta_2 = \arctan \left((b^2/a) \sqrt{D_{\text{ME}}^2 - b^2} \right)$ is the angle of the tangent point and x - y plane. This equation shows that when the distance goes to infinity, the angle θ_2 will approach 90° . Equation (9) will then equal half of Equation (7), meaning that half of the Earth will be observed in an extreme situation. For simplification, in previous studies the Earth has been treated as a sphere with a radius $a = b = \rho_E$, wherein the visible area S_{sphere} of the Earth from a sensor could be derived as

$$S_{\text{sphere}} = 2\pi \rho_E^2 \left(1 - \frac{\rho_E}{D_{\text{ME}}} \right) \quad (10)$$

The above equation could be obtained by substituting $a = b = \rho_E$ into Equation (8) as well, indicating that the spherical assumption is a special case for an ellipsoid, and that the greater the eccentricity of the ellipsoid, the larger the difference between the spherical assumption and the ellipsoid situation of the Earth.

3. Results and discussion

The observational capabilities of Moon-based Earth observation platforms are mainly determined by the relative positions of the Moon and the Earth. However, the observation geometry is determined not only by these relative positions, but also by the polar motion of the Earth, the libration of the Moon, and the shapes of the Earth and Moon. To quantify

Figure 5(a–c) show the sensitivity factors of Equation (4) for the target position of the vector $t = (x_t, y_t, z_t)$ with respect to each of the coordinate components of the sensor position $p = (x_p, y_p, z_p)$. These figures reveal that there were several characteristics of the fractional uncertainties associated with the sensor position. First, the uncertainties of the target position and the uncertainties of the sensor position exhibited nearly the same scale, which suggests that the lunar orbit error may cause small errors in the target position. The second characteristic was that the error of the sensor position along one axis can cause errors for every direction of the target position, indicating that the error in one direction will propagate in other directions. Figure 6(a–c) show the sensitivity factors of Equation (5) of the looking vector $\hat{l} = (m, n, q)$ with respect to each of the coordinate components of the sensor position. The figures show that the uncertainties of the target position due to uncertainties of the looking vector were much larger than those of the sensor position; the scale of these uncertainties was about 10^7 to 10^8 . These findings

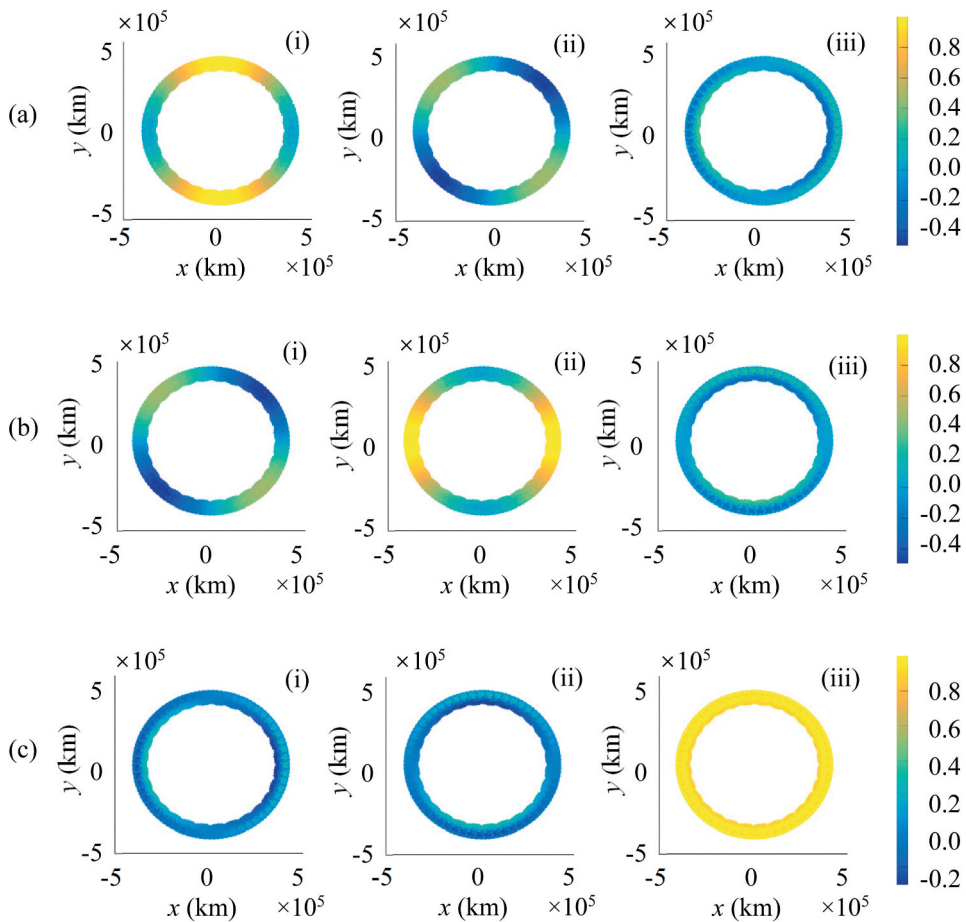


Figure 5. Sensitive factors of the sensor position to the components of the intersection position. (a) x -component of the intersection position. (b) y -component of the intersection position. (c) z -component of the intersection position. For each intersection component, the x - (i), y - (ii), and z - (iii) components of the sensor positions are given.

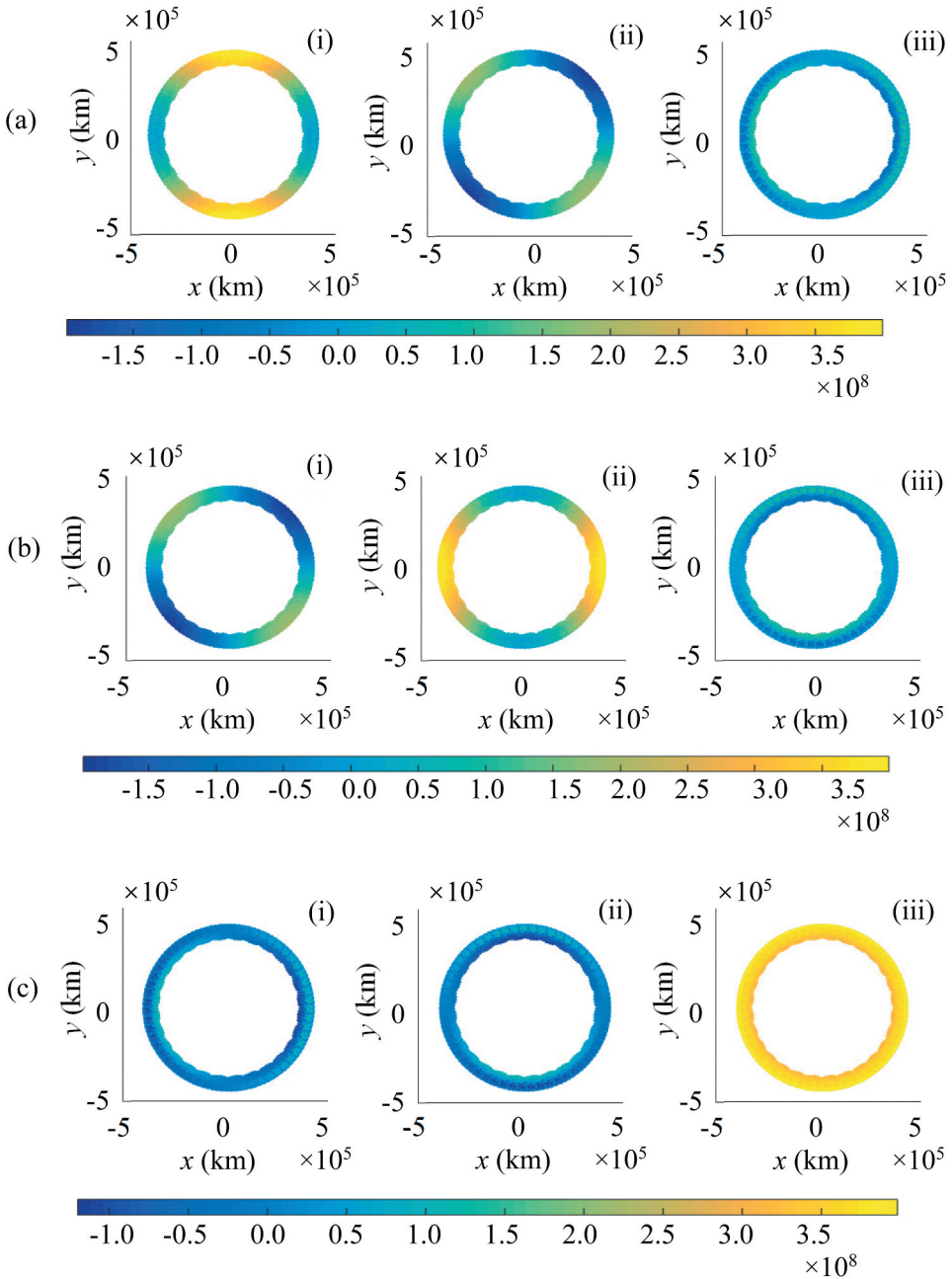


Figure 6. Sensitive factors of the line of sight (LOS) position to the components of the intersection position. (a) x-component of the LOS vector. (b) y-component of the LOS vector. (c) z-component of the LOS vector. For each intersection component, the x- (i), y- (ii), and z- (iii) components of the LOS vector are given.

suggest that a small angle error can cause a large position error of the target on Earth. Moreover, the angular accuracy of the Moon-based sensor presents a critical challenge

that must be solved to enable an on-orbit geolocation. This is especially important for SAR imaging, as the range history and focus plane are very important for SAR focusing.

In addition to the temporal changes of the sensitive factors, another important phenomenon in Earth observation is spatial variability. The sensitive factors calculated using the equations in the supplemental material, in which the target is located at different places on the Earth's surface, and the Moon is located on the x -axis (i.e., the LOS vector is along x -axis), are shown in Figure 7. The figure shows that for most of the positions, the sensitive factors $\partial t_z / \partial \hat{l}_z$ and $\partial t_y / \partial \hat{l}_y$ are larger than $\partial t_x / \partial \hat{l}_x$. This is because the LOS vector is along the x -axis, so the change in the x -component of the LOS vector will have less impact on the x -component of the location of the target. Additionally, if the Earth is a sphere, then after a 90° rotation, the sensitive factors $\partial t_x / \partial \hat{l}_y$ and $\partial t_x / \partial \hat{l}_z$ will be

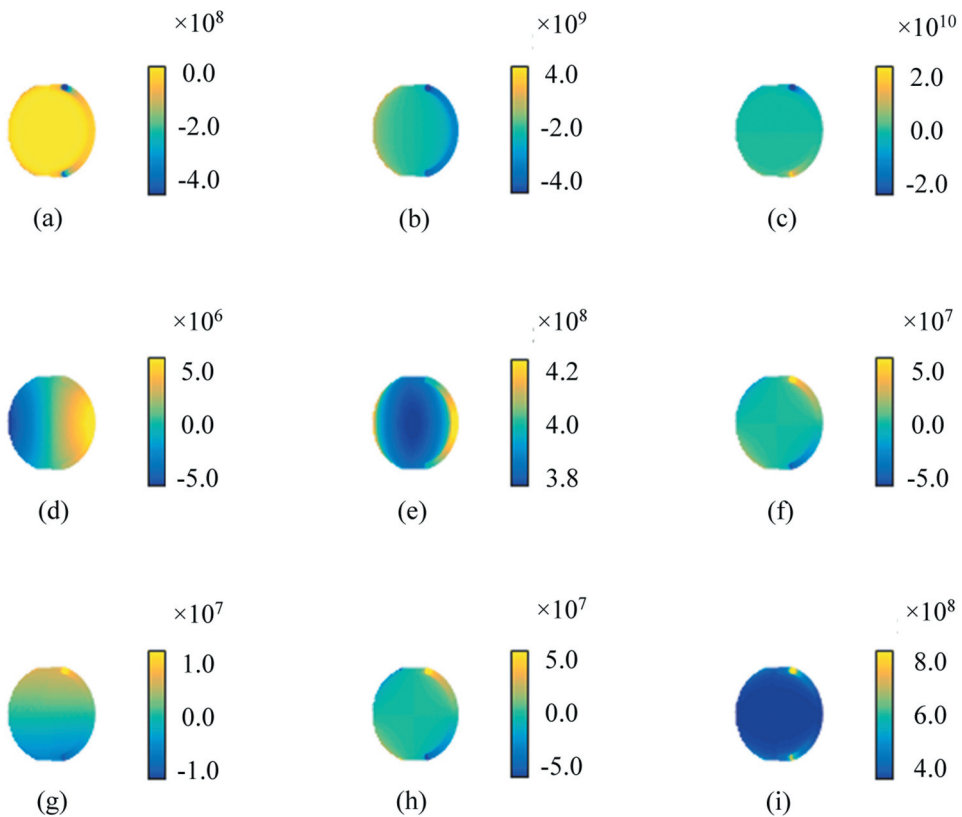


Figure 7. Spatial variability of the sensitive factors of the components of the LOS vector to the components of the intersection position. (a) x component of the LOS to the x component of the position. (b) y component of the LOS to the x component of the position. (c) z component of the LOS to the x component of the position. (d) x component of the LOS to the y component of the position. (e) y component of the LOS to the y component of the position. (f) z component of the LOS to the y component of the position. (g) x component of the LOS to the z component of the position. (h) y component of the LOS to the z component of the position. (i) z component of the LOS to the z component of the position.

equal. This was also tested via simulation; however, we found that the y - and z -components of the LOS vector impact to the position of the target $\partial t_x / \partial \hat{l}_y$ and $\partial t_x / \partial \hat{l}_z$ was not rotationally equal, as the lengths of the ellipsoid semi-axes differed.

3.2. Visible area and optimum radius analysis

The visible area of the Earth is an important parameter for Earth observation. It denotes the capability of the observation platform, and the visible area is determined by the geometric shape of the Earth and the position of the observer. The visible area of the Moon-based sensor has been discussed assuming a spherical Earth (Ren et al. 2017a; Ye et al. 2017). For the Earth ellipsoid, such as that used in GRS 80, the analytical form of the visible area from the sensor could be obtained only when it is placed on a polar axis. For sensors located on the equatorial plane of the Earth, the visible area could only be obtained using series expansion. Due to the difficulties in obtaining the visible area for the Earth ellipsoid, the alternative, which assumes sphericity, is also feasible. However, the radius of the Earth then becomes a critical parameter for determining the visible area. There are several possible methods to define the radius of a spherical Earth, such as using the length of semi-axes or the mean value of them. In this study, we further analysed the optimum radius of a spherical Earth for Moon-based Earth observations that could achieve a visible area as accurate as that of the ellipsoid.

In contrast to the spherical assumption, for an ellipsoid Earth, the visible area of the sensor could only be obtained in special cases. Considering that the Moon is always near the equatorial plane of the Earth, it is reasonable to set the sensor on the equatorial plane of the Earth. For the reference system, we consider GRS 80, which was suggested by the International Astronomical Union (IAU). The semi-major axis was $a = 6.378 \times 10^6$ m around the equator, and the semi-minor axis was $b = 6.357 \times 10^6$ m along the polar axis. Six types of radii were defined for comparison. The first radius type was defined as the length of the semi-major axis, which was denoted as $\bar{\rho}_1 = a$; the second type was defined as the length of the semi-minor axis, denoted as $\bar{\rho}_2 = b$. The third radius type was defined as the arithmetic mean of the semi-axis, which was denoted as $\bar{\rho}_3 = (a + b)/2$; the fourth type was defined as the geometric mean of the semi-axis, denoted as $\bar{\rho}_4 = \sqrt{ab}$. The fifth radius type was defined as the area of the sphere equal to the ellipsoid, which was denoted as $\bar{\rho}_5 = \sqrt{A/4\pi}$, where A is the area which obtained from equation (7); the sixth type was defined as the volume of the sphere equal to the ellipsoid, denoted as $\bar{\rho}_6 = \sqrt[3]{a^2b}$. The visible area of the GRS 80 ellipsoid from the sensor was computed with series expansion.

As the distance from the Moon to the Earth is about 350,000 to 400,000 km, different types of radii were computed, and the visible area is plotted in Figure 8. It is clear that the visible areas of the different types of radii were between the limits of type and \bar{r}_2 , while the visible areas for the types of radii defined as the arithmetic and geometrical mean of the semi-axis were smaller than those for the real situation. The closest situation was the sixth, followed by the fifth radius type. Figure 8(b) shows more details for the real situation and type five and six. The radius could be adjusted to meet the real situation, and after some simple derivation, the optimum radius could be written as a function of the distance between the Earth and the Moon

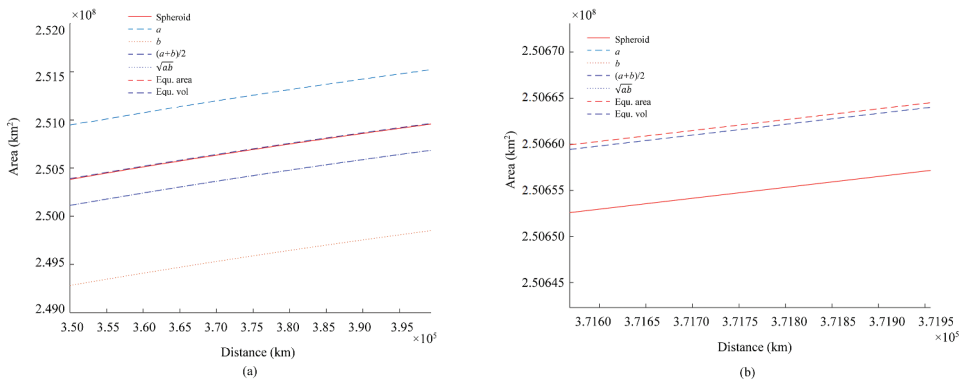


Figure 8. (a) Area comparison between different radius definitions. (b) The magnified plot near 2.506×10^8 .

$$\rho = 6370719.3436 + 7.817 \times 10^{-7} D_{ME} - 7.0104 \times 10^{-16} D_{ME}^2 \quad (11)$$

The first term on the left side is the constant which denotes the median value between the length of the semi major axis and minor axis, the linear term shows that the optimum radius is related to the distance between the Earth and the Moon, and the third term is a small adjustment. Considering that the distance between the Earth and the Moon is temporally changing, the above function is always time related and will make the visible area accurate for Moon based Earth observations.

4. Conclusions

China's Chang'e-4 relay satellite, named Magpie Bridge, has been successfully launched on 21 May 2018, and Moon-based Earth observation platforms will be constructed in the near future as one sub task of the follow-up lunar mission of China. This study focused on the characteristics of Moon-based Earth observation platforms relative to an ellipsoid Earth. Our work employs an underlying geometry that differs from that used in previous studies with spherical assumptions, and can, thus, describe the Earth's shape more accurately. Furthermore, the explicit expression of the sensitive factors of the LOS and sensor position to the intersection point of the LOS vector and the Earth ellipsoid are given. Our findings suggest that, although Moon-based Earth observations could obtain a full view of the Earth with a small view angle, more accurate angular control is needed to ensure a precise geolocation. Furthermore, different from studies that assumed a spherical Earth, the visible area of the sensor for an ellipsoid Earth could only be obtained in special cases. In such cases, the optimized radius for computing the visible area of the Earth from the Moon may be obtained as a function of the distance between the Earth and the Moon. Moon-based Earth observation is a new area of study, and while several questions remain, this study provides another step that may further advance the development and understanding of future Moon-based Earth

observation systems.

Acknowledgements

The JPL Development Ephemeris has been downloaded free of charge from <https://ssd.jpl.nasa.gov/>. The authors would like to thank the anonymous reviewers whose remarks provided valuable improvements.

Disclosure statement

No potential conflict of interest was reported by the authors.

Funding

This work was supported by the National Science Foundation of China [41590852], the National Key Research and Development Program of China [2020YFE0202100] and the Key Research Program of Frontier Sciences, CAS [QYZDY-SSW-DQC026].

ORCID

Guang Liu  <http://orcid.org/0000-0001-8596-8528>

Huadong Guo  <http://orcid.org/0000-0001-5954-2179>

Ramon F. Hanssen  <http://orcid.org/0000-0002-6067-7561>

References

- Andrew, M. E. 2015. "Earth Observation of Ecosystem Services." *African Journal of Range & Forage Science* 32 (1): 70–71. doi: [10.2989/10220119.2014.946537](https://doi.org/10.2989/10220119.2014.946537).
- Archinal, B. A., M. F. A'Hearn, E. Bowell, A. Conrad, G. J. Consolmagno, R. Courtin, T. Fukushima, et al. 2011. "Report of the IAU Working Group on Cartographic Coordinates and Rotational Elements: 2009." *Celestial Mechanics and Dynamical Astronomy* 109 (2): 101–135. doi: [10.1007/s10569-010-9320-4](https://doi.org/10.1007/s10569-010-9320-4).
- Bendek, E. A., R. Belikov, J. Lozi, S. Thomas, J. Males, S. Weston, and M. McElwain. 2015. *Space Telescope Design to Directly Image the Habitable Zone of Alpha Centauri*, edited by S. Shaklan, 960516. doi: [10.1117/12.2188999](https://doi.org/10.1117/12.2188999).
- Blair, D. M., L. Chappaz, R. Sood, C. Milbury, A. Bobet, H. J. Melosh, K. C. Howell, and A. M. Freed. 2017. "The Structural Stability of Lunar Lava Tubes." *Icarus* 282 (January): 47–55. doi: [10.1016/j.icarus.2016.10.008](https://doi.org/10.1016/j.icarus.2016.10.008).
- Carruthers, G. R., and T. Page. 1972. "Apollo 16 Far-Ultraviolet Camera/Spectrograph: Earth Observations." *Science* 177 (4051): 788–791. doi: [10.1126/science.177.4051.788](https://doi.org/10.1126/science.177.4051.788).
- Carruthers, G. R., and T. Page. 1976. "Apollo 16 Far Ultraviolet Spectra of the Terrestrial Airglow." *Journal of Geophysical Research* 81 (10): 1683–1694. doi: [10.1029/JA081i010p01683](https://doi.org/10.1029/JA081i010p01683).
- Chovitz, B. H. 1981. "Modern Geodetic Earth Reference Models." *Eos, Transactions American Geophysical Union* 62 (7): 65. doi: [10.1029/EO062i007p00065](https://doi.org/10.1029/EO062i007p00065).
- Chuvieco, E., ed. 2008. *Earth Observation of Global Change*. Dordrecht: Springer Netherlands. doi: [10.1007/978-1-4020-6358-9](https://doi.org/10.1007/978-1-4020-6358-9).
- Clarke, A. R. 1878. "XII. On the Figure of the Earth." *Philosophical Magazine Series 5* 6 (35): 81–93. doi: [10.1080/14786447808639480](https://doi.org/10.1080/14786447808639480).
- Ding, Y., H. Guo, G. Liu, C. Han, H. Shang, Z. Ruan, and M. Lv. 2019. "Constructing a High-Accuracy Geometric Model for Moon-Based Earth Observation." *Remote Sensing* 11 (22): 2611. doi: [10.3390/rs11222611](https://doi.org/10.3390/rs11222611).

- Folkner, W. M., J. G. Williams, and D. H. Boggs. 2009. *The Planetary and Lunar Ephemeris DE 421*. IPN Progress Report 42-178.
- Fornaro, G., G. Franceschetti, F. Lombardini, A. Mori, and M. Calamia. 2010. "Potentials and Limitations of Moon-Borne SAR Imaging." *IEEE Transactions on Geoscience and Remote Sensing* 48 (7): 3009–3019. doi: [10.1109/TGRS.2010.2041463](https://doi.org/10.1109/TGRS.2010.2041463).
- Goodchild, M. F., H. Guo, A. Annoni, L. Bian, K. de Bie, F. Campbell, M. Craglia, et al. 2012. "Next-Generation Digital Earth." *Proceedings of the National Academy of Sciences* 109 (28): 11088–11094. doi: [10.1073/pnas.1202383109](https://doi.org/10.1073/pnas.1202383109).
- Gowing, R. 1983. *Roger Cotes, Natural Philosopher*. Cambridge [Cambridgeshire]; New York: Cambridge University Press.
- Grafarend, E. W., M. Klapp, and Z. Martinec. 2010. "Spacetime Modeling of the Earth's Gravity Field by Ellipsoidal Harmonics." In *Handbook of Geomathematics*, edited by M. Willi Freeden, Z. Nashed, and T. Sonar, 159–252. Berlin, Heidelberg: Springer Berlin Heidelberg. doi: [10.1007/978-3-642-01546-5_7](https://doi.org/10.1007/978-3-642-01546-5_7).
- Guo, H. 2009. "Space-Based Observation for Sensitive Factors of Global Change." *Bulletin of the Chinese Academy of Sciences* 23 (4): 226–228.
- Guo, H., C. Dou, X. Zhang, C. Han, and X. Yue. 2016a. "Earth Observation from the Manned Low Earth Orbit Platforms." *ISPRS Journal of Photogrammetry and Remote Sensing* 115 (May): 103–118. doi: [10.1016/j.isprsjprs.2015.11.004](https://doi.org/10.1016/j.isprsjprs.2015.11.004).
- Guo, H., G. Liu, and Y. Ding. 2017. "Moon-Based Earth Observation: Scientific Concept and Potential Applications." *International Journal of Digital Earth* July, 1–12. doi: [10.1080/17538947.2017.1356879](https://doi.org/10.1080/17538947.2017.1356879).
- Guo, H., G. Liu, Y. Ding, Y. Zou, S. Huang, L. Jiang, J. Gensuo, et al. 2016b. *Moon-Based Earth Observation for Large Scale Geoscience Phenomena*, 3705–3707. IEEE. doi: [10.1109/IGARSS.2016.7729960](https://doi.org/10.1109/IGARSS.2016.7729960).
- Hamill, P. 2007. "A Lunar Earth Observatory." In Tempe, Arizona. <http://www.lpi.usra.edu/meetings/LEA/whitepapers/HamillWhite.Paper2.pdf>.
- Hamill, P. 2016. Atmospheric Observations from the Moon: A Lunar Earth-Observatory, In 2016 IEEE International Geoscience and Remote Sensing Symposium (IGARSS), 3719–3722. Beijing, China, IEEE. doi: [10.1109/IGARSS.2016.7729964](https://doi.org/10.1109/IGARSS.2016.7729964).
- Harris, J. W., and H. Stocker. 1998. *Handbook of Mathematics and Computational Science*. New York, NY: Springer New York. doi: [10.1007/978-1-4612-5317-4](https://doi.org/10.1007/978-1-4612-5317-4).
- Herman, M., J. Y. Balois, L. Gonzalez, P. Lecomte, J. Lenoble, R. Santer, and C. Verwaerde. 1986. "Stratospheric Aerosol Observations from a Balloon-Borne Polarimetric Experiment." *Applied Optics* 25 (19): 3573. doi: [10.1364/AO.25.003573](https://doi.org/10.1364/AO.25.003573).
- Huang, S., J. Liao, J. Guang, J. Wu, S. Bi, X. Tang, and J. Kuang. 2016. Towards Moon-Based Monitoring of Energy Budget of the Earth Climate System, In 2016 IEEE International Geoscience and Remote Sensing Symposium (IGARSS), 3726–3729. Beijing, China, IEEE. doi: [10.1109/IGARSS.2016.7729966](https://doi.org/10.1109/IGARSS.2016.7729966).
- Ikeda, M., and F. Dobson, eds. 1995. *Oceanographic Applications of Remote Sensing*. Boca Raton: CRC Press.
- Jekeli, C. 2001. *Inertial Navigation Systems with Geodetic Applications*. Berlin; New York: Walter de Gruyter.
- Jiang, Z., and S. Shekhar. 2017. *Spatial Big Data Science*. New York, NY: Springer Berlin Heidelberg.
- Johnson, J. R., P. G. Lucey, T. C. Stone, and M. I. Staid. 2007. "Visible/Near-Infrared Remote Sensing of Earth from the Moon." In Tempe, Arizona. https://www.lpi.usra.edu/meetings/LEA/whitepapers/Johnson_etal_v02.pdf.
- Kaufmann, M., and R. Song. 2016. Atmospheric Gravity Waves Observation from a Lunar Base, In 2016 IEEE International Geoscience and Remote Sensing Symposium (IGARSS), 3712–3714. Beijing, China, IEEE. doi: [10.1109/IGARSS.2016.7729962](https://doi.org/10.1109/IGARSS.2016.7729962).
- Lautenbacher, C. C. 2006. "The Global Earth Observation System of Systems: Science Serving Society." *Space Policy* 22 (1): 8–11. doi: [10.1016/j.spacepol.2005.12.004](https://doi.org/10.1016/j.spacepol.2005.12.004).

- Liu, G., H. Guo, X. Wang, and L. Zhang. 2016. *Report on the Scheme and Key Technologies of Lunar Base Earth Observation*. Strategic Pioneer Program on Space Science of Chinese Academy of Sciences XDA04077200. Beijing, China: Chinese Academy of Sciences.
- May, A. 2017. "A Brief History of the Moon." *The Telescopic Tourist's Guide to the Moon: A Brief History of the Moon*. 37–56. Cham: Springer International Publishing. doi: [10.1007/978-3-319-60741-2_3](https://doi.org/10.1007/978-3-319-60741-2_3).
- McCarthy, D. D., and G. Petit. 2004. *IERS Conventions (2003)*. IERS Technical Note, No. 32. Frankfurt am Main, Germany: International Earth Rotation and Reference Systems Service (IERS).
- Moccia, A., and A. Renga. 2010. "Synthetic Aperture Radar for Earth Observation from a Lunar Base: Performance and Potential Applications." *IEEE Transactions on Aerospace and Electronic Systems* 46 (3): 1034–1051. doi: [10.1109/TAES.2010.5545172](https://doi.org/10.1109/TAES.2010.5545172).
- Moritz, H. 1980. "Geodetic Reference System 1980." *Bulletin Géodésique* 54 (3): 395–405. doi: [10.1007/BF02521480](https://doi.org/10.1007/BF02521480).
- Muironen, K., Y. Shkuratov, A. Ovcharenko, J. Piironen, D. Stankevich, O. Miloslavskaya, S. Kaasalainen, and J.-L. Josset. 2002. "The SMART-1 AMIE Experiment: Implication to the Lunar Opposition Effect." *Planetary and Space Science* 50 (14–15): 1339–1344. doi: [10.1016/S0032-0633\(02\)00128-9](https://doi.org/10.1016/S0032-0633(02)00128-9).
- NASA. 2006. "Lunar Exploration Objectives, Version 1." https://www.nasa.gov/pdf/163560main_LunarExplorationObjectives.pdf.
- Pallé, E., and P. R. Goode. 2009. "The Lunar Terrestrial Observatory: Observing the Earth Using Photometers on the Moon's Surface." *Advances in Space Research* 43 (7): 1083–1089. doi: [10.1016/j.asr.2008.11.022](https://doi.org/10.1016/j.asr.2008.11.022).
- Reid, W. V., D. Chen, L. Goldfarb, H. Hackmann, Y. T. Lee, K. Mokhele, E. Ostrom, et al. 2010. "Earth System Science for Global Sustainability: Grand Challenges." *Science* 330 (6006): 916–917. doi: [10.1126/science.1196263](https://doi.org/10.1126/science.1196263).
- Ren, Y., H. Guo, G. Liu, and H. Ye. 2017a. "Simulation Study of Geometric Characteristics and Coverage for Moon-Based Earth Observation in the Electro-Optical Region." *IEEE Journal of Selected Topics in Applied Earth Observations and Remote Sensing* 10 (6): 2431–2440. doi: [10.1109/JSTARS.2017.2711061](https://doi.org/10.1109/JSTARS.2017.2711061).
- Ren, Y., H. Guo, G. Liu, and H. Ye. 2017b. "Simulation Study of Geometric Characteristics and Coverage for Moon-Based Earth Observation in the Electro-Optical Region." *IEEE Journal of Selected Topics in Applied Earth Observations and Remote Sensing* 10 (6): 2431–2440. doi: [10.1109/JSTARS.2017.2711061](https://doi.org/10.1109/JSTARS.2017.2711061).
- Ren, Y., H. Guo, G. Liu, H. Ye, Y. Ding, D. Zhang, Z. Ruan, and M. Lv. 2016. *Simulation of Moon-Based Observation for Large-Scale Earth Science Phenomena*, 6253–6256. Beijing: IEEE. doi: [10.1109/IGARSS.2016.7730634](https://doi.org/10.1109/IGARSS.2016.7730634).
- Renga, A., and A. Moccia. 2016. Moon-Based Synthetic Aperture Radar: Review and Challenges, In 2016 IEEE International Geoscience and Remote Sensing Symposium (IGARSS), 3708–3711. Beijing, China, IEEE. doi: [10.1109/IGARSS.2016.7729961](https://doi.org/10.1109/IGARSS.2016.7729961).
- Rosenqvist, A., M. Shimada, B. Chapman, A. Freeman, G. De Grandi, S. Saatchi, and Y. Rauste. 2010. "The Global Rain Forest Mapping Project - A Review." *International Journal of Remote Sensing* 21: 1375–1387. doi: [10.1080/014311600210227](https://doi.org/10.1080/014311600210227).
- Ryerson, R. A. 1998. *Manual of Remote Sensing*, Edited by American Society for Photogrammetry and Remote Sensing, 3rd ed. New York: J. Wiley.
- Ryu, J.-H., and K. Hayhoe. 2017. "Observed and CMIP5 Modeled Influence of Large-Scale Circulation on Summer Precipitation and Drought in the South-Central United States." *Climate Dynamics* February. doi: [10.1007/s00382-017-3534-z](https://doi.org/10.1007/s00382-017-3534-z).
- Sandau, R. 2010. "Status and Trends of Small Satellite Missions for Earth Observation." *Acta astronautica* 66 (1–2): 1–12. doi: [10.1016/j.actaastro.2009.06.008](https://doi.org/10.1016/j.actaastro.2009.06.008).
- Seeber, G. 2003. *Satellite Geodesy*. 2nd completely rev. and extended ed. Berlin; New York: Walter de Gruyter.
- Skinner, B. J., and B. W. Murck. 2011. *The Blue Planet: An Introduction to Earth System Science*. 3rd ed. Hoboken, NJ: Wiley.

- Song, Y., X. Wang, S. Bi, J. Wu, and S. Huang. 2017. "Effects of Solar Radiation, Terrestrial Radiation and Lunar Interior Heat Flow on Surface Temperature at the Nearside of the Moon: Based on Numerical Calculation and Data Analysis." *Advances in Space Research* 60 (5): 938–947. doi: [10.1016/j.asr.2017.05.013](https://doi.org/10.1016/j.asr.2017.05.013).
- Stahl, H. P. 2017. Overview of a Telescope Concept Design for the Habitable-Zone Exoplanet Direct Imaging Mission, In Proc. SPIE 10398, UV/Optical/IR Space Telescopes and Instruments: Innovative Technologies and Concepts VIII, edited by H. A. MacEwen and J. B. Breckinridge, 1039806. San Diego, California, United States. SPIE Digital Library. doi: [10.1117/12.2275192](https://doi.org/10.1117/12.2275192).
- Stammer, D., and A. Cazenave, eds. 2017. *Satellite Altimetry over Oceans and Land Surfaces*. Boca Raton, FL: Taylor & Francis.
- Taylor, G. J. 1988. Future Astronomical Observatories on the Moon: Geological Considerations for Lunar Telescopes. Proceeding of a workshop jointly sponsored by the American Astronomical Society. Houston, Texas, USA. 21–30. NASA Conference Publication 2489.
- Torge, W., and J. Müller. 2012. "Geodesy." In *De Gruyter Textbook*. 4th ed. Berlin; Boston: De Gruyter.
- Vömel, H. 2002. "Balloon-Borne Observations of Water Vapor and Ozone in the Tropical Upper Troposphere and Lower Stratosphere." *Journal of Geophysical Research* 107: D14. doi: [10.1029/2001JD000707](https://doi.org/10.1029/2001JD000707).
- Wu, K., C. Ji, L. Luo, and X. Wang. 2020. "Simulation Study of Moon-Based InSAR Observation for Solid Earth Tides." *Remote Sensing* 12 (1): 123. doi: [10.3390/rs12010123](https://doi.org/10.3390/rs12010123).
- Xu, Z., and K.-S. Chen. 2018. "On Signal Modeling of Moon-Based Synthetic Aperture Radar (SAR) Imaging of Earth." *Remote Sensing* 10 (3): 486. doi: [10.3390/rs10030486](https://doi.org/10.3390/rs10030486).
- Xu, Z., and K.-S. Chen. 2019. "Effects of the Earth's Curvature and Lunar Revolution on the Imaging Performance of the Moon-Based Synthetic Aperture Radar." *IEEE Transactions on Geoscience and Remote Sensing* 57 (8): 5868–5882. doi: [10.1109/TGRS.2019.2902842](https://doi.org/10.1109/TGRS.2019.2902842).
- Xu, Z., K.-S. Chen, and G. Zhou. 2019. "Zero-Doppler Centroid Steering for the Moon-Based Synthetic Aperture Radar: A Theoretical Analysis." *IEEE Geoscience and Remote Sensing Letters* 1–5. doi: [10.1109/LGRS.2019.2941505](https://doi.org/10.1109/LGRS.2019.2941505).
- Yamazaki, J., S. Mitsuhashi, M. Yamauchi, J. Tachino, R. Honda, M. Shirao, K. Tanimoto, et al. 2010. "High-Definition Television System Onboard Lunar Explorer Kaguya (SELENE) and Imaging of the Moon and the Earth." *Space Science Reviews* 154 (1–4): 21–56. doi: [10.1007/s11214-010-9697-0](https://doi.org/10.1007/s11214-010-9697-0).
- Ye, H., H. Guo, G. Liu, Q. Guo, and J. Huang. 2018a. "Looking Vector Direction Analysis for the Moon-Based Earth Observation Optical Sensor." *IEEE Journal of Selected Topics in Applied Earth Observations and Remote Sensing* 11 (11): 4488–4499. doi: [10.1109/JSTARS.2018.2870247](https://doi.org/10.1109/JSTARS.2018.2870247).
- Ye, H., H. Guo, G. Liu, Q. Guo, and J. Huang. 2018b. "Looking Vector Direction Analysis for the Moon-Based Earth Observation Optical Sensor." *IEEE Journal of Selected Topics in Applied Earth Observations and Remote Sensing* 11 (11): 4488–4499. doi: [10.1109/JSTARS.2018.2870247](https://doi.org/10.1109/JSTARS.2018.2870247).
- Ye, H., H. Guo, G. Liu, and Y. Ren. 2017. "Observation Scope and Spatial Coverage Analysis for Earth Observation from a Moon-Based Platform." *International Journal of Remote Sensing* October, 1–25. doi: [10.1080/01431161.2017.1395976](https://doi.org/10.1080/01431161.2017.1395976).
- Ye, H., H. Guo, G. Liu, and Y. Ren. 2018. "Observation Scope and Spatial Coverage Analysis for Earth Observation from a Moon-Based Platform." *International Journal of Remote Sensing* 39 (18): 5809–5833. doi: [10.1080/01431161.2017.1395976](https://doi.org/10.1080/01431161.2017.1395976).
- Ye, H., H. Guo, G. Liu, Y. Ren, Y. Ding, and M. Lv. 2016. *Coverage Analysis on Global Change Sensitive Regions from Moon Based Observation*, 3734–3737. Beijing: IEEE. doi: [10.1109/IGARSS.2016.7729968](https://doi.org/10.1109/IGARSS.2016.7729968).
- Zhang, D. 2012. "Study on Methodology of Lunar-Based Earth Observation for Global Change." Master Thesis, Shanghai: East China Normal University.
- Zheng, Y., Z. Ouyang, C. Li, J. Liu, and Y. Zou. 2008. "China's Lunar Exploration Program: Present and Future." *Planetary and Space Science* 56 (7): 881–886. doi: [10.1016/j.pss.2008.01.002](https://doi.org/10.1016/j.pss.2008.01.002).